Cyclotron–phonon resonance line-width in monolayer silicene

Le T.T. Phuong [a], Bui D. Hoi [a], Pham V. Dung [a,b], Nguyen N. Hieu [c], Chuong V. Nguyen [d], Huynh V. Phuc [e], Nguyen T. Dung [f], Pham D. Khang [g,h,*]

[a] *Department of Physics and Center for Theoretical and Computational Physics, University of Education, Hue University, Hue, Viet Nam*
[b] *Nguyen Hue University, Dong Nai Province, Viet Nam*
[c] *Institute of Research and Development, Duy Tan University, Danang, Viet Nam*
[d] *Department of Materials Science and Engineering, Le Quy Don Technical University, Ha Noi, Viet Nam*
[e] *Division of Theoretical Physics, Dong Thap University, Dong Thap, Viet Nam*
[f] *Vinh University, Nghe An Province, Viet Nam*
[g] *Laboratory of Applied Physics, Advanced Institute of Materials Science, Ton Duc Thang University, Ho Chi Minh City, Viet Nam*
[h] *Faculty of Applied Sciences, Ton Duc Thang University, Ho Chi Minh City, Viet Nam*

ARTICLE INFO

ABSTRACT

We theoretically observe the cyclotron–phonon resonance (CPR) in monolayer silicene by considering the magneto-optical absorption power (AP) of the system. The AP is calculated utilising the projection operator technique when a static magnetic field is subjected perpendicularly to the plane of the material and the electron–optical phonon scattering is involved. The absorption spectra show the resonance behaviour where the photon energies at resonant peaks satisfy the cyclotron–phonon (CPR) conditions in which the CPR energy depends linearly on the square root of the magnetic field strength. This dependence is similar to that in graphene and different from that in monolayer MoS_2 and conventional low-dimensional semiconductors. The dependence of the full-width at half maximum (FWHM) on the magnetic field strength has the laws similar to those obtained for graphene and monolayer MoS_2. However, the FWHM value in silicene is two times smaller than it is in graphene and has the same order as it does in monolayer MoS_2. At relatively high temperature ($T > 300$ K), the FWHM for phonon emission differs very little from that for phonon absorption and becomes identical in two cases when $T > 350$ K.

1. Introduction

Silicene is an analogue of graphene in which silicon atoms deposited in a two-dimensional (2D) hexagonal lattice [1–9]. Similar to graphene, silicene possesses fascinating physical properties [1]. For example, charged carriers (electrons and holes) in silicene obey relativistic Dirac equation for massless fermions and their electronic dispersion is linear around the Dirac points. That results in a high carrier mobility in silicene. Also, the quantum spin Hall effect can be observed in silicene [10]. Beside those graphene-like properties, silicene itself has some distinct properties. The outer-shell electrons in silicene have the weak π bonding that makes silicene to have a low-buckled structure [9]. The band gap of the material can be controlled by applied electric field or magnetic fields. Also, silicene has a small band gap of about 1.55 meV [8,10]. More importantly, compared with graphene, silicene is more advantageous for instant nanoelectronic applications because it is compatible with existing nanoelectronic devices which are based on silicon technology. That is the reason that silicene has been being paid much attention recently.

For a material subjected to a uniform static magnetic field and an optical field (electromagnetic wave) simultaneously, under certain conditions the cyclotron resonance (CR) can be observed. The CR occurs when the magneto-optical absorption of carriers (electrons or holes) satisfies the condition $M\omega_c = \omega$, where ω_c and ω are, respectively, the cyclotron frequency and photon frequency, and M is an integer. If the emission or absorption of an optical phonon goes with the CR, there occurs the so-called phonon-assisted CR or cyclotron–phonon resonance (CPR). Both CR and CPR have been shown to have many applications in solid state research such as determining of the carrier effective mass, the phonon energy, the difference between Landau energy levels, the mechanism of carrier–phonon scattering, and some other parameters [11]. On the other hand, studies have shown that the transport properties in materials at high temperatures are strongly influenced by electron–phonon interaction. At relatively high temperatures ($T > 50$ K), the electron–optical phonon interaction dominates and gives a major contribution to the electron transition in comparison with other interactions. Therefore, the CPR is usually observed at high temperatures when the emission or absorption of optical phonon is evident. Studies on the CPR have been performed widely in three-dimensional (3D) and conventional low-dimensional electrons systems [11–28]. For advanced atomically thin materials, in particular, the CPR has been also investigated very recently in graphene [17,18,29,30] and monolayer molybdenum disulphide [31,32]. For silicene-based materials, there have been some studies on the optical absorption considering separately the effects of optical field, dc electric field, exchange field [33], substrate [34], and static magnetic field [35]. However, the combined effect of a static magnetic field and the electron–phonon coupling on the optical absorption in silicene has not considered and, hence, the CPR has not been investigated theoretically in the material.

Motivated by the fascinating properties of silicene and earlier studies on the CPR effect in other low-dimensional materials, in the present study we theoretically investigate the absorption of an optical field by monolayer silicene in the presence of a perpendicular static magnetic field. The electron–phonon interaction in the material is taken into account at high temperatures. The main purposes is to check the magneto-optical absorption behaviours of silicene and make a comparison with the other similar 2D structures such as graphene and MoS$_2$ monolayer. In particular, the absorption power (AP) is calculated using the projection operator technique which was used successfully in some works [32,36]. The AP obtained by this method has been shown to contain full electron states during the transport process, including the initial, final and mediate states [36]. Therefore, one can extract and examine possible transitions of electrons in the considered phenomenon. The paper is organised as follows. In Section 2, we introduce the theoretical model and the obtained analytical results. Section 3 presents numerical results and discussion. Finally, some concluding remarks are shown in Section 4.

2. Theoretical model and analytical results

In this investigation, we adopt the model of a silicene sheet in a perpendicular static magnetic field $\vec{B}$ as introduced in Ref. [37]. The electron energy is then quantised completely into Landau levels and given by

$$E^{\pm}_{n,s_z,p} = p\hbar\omega_c \left\{ n + \left[\bar{\lambda}_{\pm}(s_z) \right]^2 \right\}^{1/2}, \tag{1}$$

where the upper sign (+) is for the K valley and the lower sign (−) is for the K' valley; $n = 0, 1, 2, \ldots$ is the Landau level index; $s_z = +1$ (−1) for up (down) spin; $p = +1$ (−1) corresponds to conduction (valence) band; $\omega_c = \sqrt{2}v_F/\ell_B$ with $\ell_B = \sqrt{\hbar/eB}$, v_F being the Fermi velocity of electron in silicene and e its absolute charge; $\bar{\lambda}_{\pm}(s_z) = \mp\lambda_{SO}s_z/\hbar\omega_c$ where λ_{SO} is the magnitude of the intrinsic spin–orbit interaction (SOI) in silicene. Here, we neglect the Rashba SOI because it was shown to be about ten times weaker than the intrinsic SOI [38].

When the above silicene sheet is further illuminated by an intense EMW, the EMW absorption power (AP) by electrons in the system can be written as

$$P(\omega) = (E_0^2/2)\text{Re}\{\sigma_{+-}(\omega)\}, \tag{2}$$

where E_0 and ω are, respectively, the amplitude and the frequency of the EMW; $\text{Re}\{\sigma_{+-}(\omega)\}$ is the real part of the magneto-optical conductivity, $\sigma_{+-}(\omega)$. According to the Kubo formalism [36]

$$\text{Re}\{\sigma_{+-}(\omega)\} = \frac{1}{\omega_c} \sum_{\alpha} \frac{|j_\alpha^+|^2 [f(E_\alpha) - f(E_{\alpha+1})] B_\alpha(\omega)}{\left[\hbar\omega - (E_{\alpha+1} - E_\alpha) \right]^2 - B_\alpha^2(\omega)}. \tag{3}$$

Here, $|\alpha\rangle \equiv |n, s_z, p\rangle$ presents the electron state; j_α^+ is the current matrix element induced by the transition of an electron between the states $|\alpha\rangle$ and $|\alpha + 1\rangle \equiv |n + 1, s_z, p\rangle$, given by $j_\alpha^+ = \langle \alpha + 1|j^+|\alpha\rangle$ with j^+ being the one-particle current operator, $j^+ = j_x + ij_y$; $f(E_\alpha) = \{\exp[(E_\alpha - E_F)/(k_BT)] + 1\}^{-1}$ is the Fermi–Dirac distribution for fermions having energy of E_α ($E_\alpha \equiv E^{\pm}_{n,s_z,p}$), where E_F is the Fermi level and T the temperature of the system. The term $B_\alpha(\omega)$ is known as the collision factor or the line-shape function which depends on the carrier scattering mechanism. In this work, we assume that the carriers in silicene are mainly scattered by optical phonons at high temperatures. Performing straightforward calculations as in the previous work [32], one can obtain the explicit expression of $B_\alpha(\omega)$ at the K valley as

$$B_\alpha(\omega) = \frac{|g_{q,\nu}|^2 S_0^2}{8\pi^2 \hbar \ell_B^4 [f(E_\alpha) - f(E_{\alpha+1})]} \left[B_1 + B_2 + B_3 + B_4 + B_5 + B_6 + B_7 + B_8 \right], \tag{4}$$

where,

$$B_1 = (1 + N_{q,\nu}) \sum_{n' \neq n} \sum_{s_z'} I^+_{n,p,n',p'}(s_z) f(E^+_{n,s_z,p})(1 - f(E^+_{n',s_z',p'}))$$

$$\times \, \delta(\hbar\omega + E^+_{n,s_z,p} - E^+_{n',s'_z,p'} - \hbar\omega_{q,\nu}), \tag{5}$$

$$B_2 = -N_{q,\nu} \sum_{n' \neq n} \sum_{s'_z,p'} I^+_{n,p,n',p'}(s_z) f(E^+_{n',s'_z,p'})(1 - f(E^+_{n,s_z,p}))$$

$$\times \, \delta(-\hbar\omega + E^+_{n,s_z,p} - E^+_{n',s'_z,p'} + \hbar\omega_{q,\nu}), \tag{6}$$

$$B_3 = N_{q,\nu} \sum_{n' \neq n} \sum_{s'_z,p'} I^+_{n,p,n',p'}(s_z) f(E^+_{n,s_z,p})(1 - f(E^+_{n',s'_z,p'}))$$

$$\times \, \delta(\hbar\omega + E^+_{n,s_z,p} - E^+_{n',s'_z,p'} + \hbar\omega_{q,\nu}) \tag{7}$$

$$B_4 = -(1 + N_{q,\nu}) \sum_{n' \neq n} \sum_{s'_z,p'} I^+_{n,p,n',p'}(s_z) f(E^+_{n',s'_z,p'})(1 - f(E^+_{n,s_z,p}))$$

$$\times \, \delta(-\hbar\omega + E^+_{n,s_z,p} - E^+_{n',s'_z,p'} - \hbar\omega_{q,\nu}), \tag{8}$$

$$B_5 = (1 + N_{q,\nu}) \sum_{n' \neq n+1} \sum_{s'_z,p'} I^+_{n+1,p,n',p'}(s_z) f(E^+_{n',s'_z,p'})(1 - f(E^+_{n+1,s_z,p}))$$

$$\times \, \delta(\hbar\omega + E^+_{n+1,s_z,p} - E^+_{n',s'_z,p'} - \hbar\omega_{q,\nu}), \tag{9}$$

$$B_6 = -N_{q,\nu} \sum_{n' \neq n+1} \sum_{s'_z,p'} I^+_{n+1,p,n',p'}(s_z) f(E^+_{n+1,s_z,p})(1 - f(E^+_{n',s'_z,p'}))$$

$$\times \, \delta(-\hbar\omega + E^+_{n+1,s_z,p} - E^+_{n',s'_z,p'} + \hbar\omega_{q,\nu}), \tag{10}$$

$$B_7 = N_{q,\nu} \sum_{n' \neq n+1} \sum_{s'_z,p'} I^+_{n+1,p,n',p'}(s_z) f(E^+_{n',s'_z,p'})(1 - f(E^+_{n+1,s_z,p}))$$

$$\times \, \delta(\hbar\omega + E^+_{n+1,s_z,p} - E^+_{n',s'_z,p'} + \hbar\omega_{q,\nu}), \tag{11}$$

$$B_8 = -(1 + N_{q,\nu}) \sum_{n' \neq n+1} \sum_{s'_z,p'} I^+_{n+1,p,n',p'}(s_z) f(E^+_{n+1,s_z,p})(1 - f(E^+_{n',s'_z,p'}))$$

$$\times \, \delta(-\hbar\omega + E^+_{n+1,s_z,p} - E^+_{n',s'_z,p'} - \hbar\omega_{q,\nu}). \tag{12}$$

Here, $N_{q,\nu}$ is the distribution function for phonons of the angular frequency $\omega_{q,\nu}$ and the wave number q in the ν mode; $g_{q,\nu}$ is the coupling matrix between electrons and optical phonons. As an examination, in this calculation we consider only the deformation potential coupling within the zeroth order, i.e, $|g_{q,\nu}|^2 = (D_t K)^2 \hbar/(2\rho\omega_{q,\nu}S_0)$ [39], where $(D_t K)^2 = 2.6 \times 10^8$ eV/cm is the optical deformation potential, ρ the 2D density of mass of the material, and S_0 the normalisation area; and

$$I^+_{n,p,n',p'}(s_z) = (\eta^+_1 \eta'^+_1)^2 + (\eta^+_2 \eta'^+_2)^2, \tag{13}$$

$$\eta^+_1 = \left[\frac{-\lambda_{SO}s_z + E^+_{n,s_z,p}}{2E^+_{n,s_z,p}}\right]^{1/2}, \tag{14}$$

$$\eta^+_2 = -p\left[\frac{\lambda_{SO}s_z + E^+_{n,s_z,p}}{2E^+_{n,s_z,p}}\right]^{1/2}, \tag{15}$$

$$\eta'^+_1 = \left[\frac{-\lambda_{SO}s_z + E^+_{n',s'_z,p'}}{2E^+_{n',s'_z,p'}}\right]^{1/2}, \tag{16}$$

$$\eta'^+_2 = -p\left[\frac{\lambda_{SO}s_z + E^+_{n',s'_z,p'}}{2E^+_{n',s'_z,p'}}\right]^{1/2}. \tag{17}$$

The physical meaning of the terms in $B(\omega)$ can be explained similarly as in Ref. [32]. In the following, the optical phonons are assumed to be dispersionless, i.e, $\omega_{q,\nu}$ and $N_{q,\nu}$ are independent of q. We also replace phenomenologically the delta functions in B_1 to B_8 by the Lorentzians to avoid the divergence, namely [40],

$$\delta(X) = \frac{1}{\pi} \frac{\hbar\gamma^{\pm}_{\alpha,\beta}}{[X^2 + \hbar^2(\gamma^{\mp}_{\alpha,\beta})^2]}, \tag{18}$$

with

$$(\gamma^{\pm}_{\alpha,\beta})^2 = \frac{g_{q,\nu}S_0}{(2\pi\hbar\ell_B)^2}\left(N_{q,\nu} \pm \frac{1}{2} + \frac{1}{2}\right)\left[(\eta^+_1 \eta'^+_1)^2 + (\eta^+_2 \eta'^+_2)^2\right]. \tag{19}$$

The results for the K' valley can be obtained by replacing $E^+_{n,s_z,p}$ by $E^-_{n,s_z,p}$, η^+_1 by η^-_1, and η^+_2 by η^-_2 in the above expressions, with

$$\eta^-_1 = -p\left[\frac{\lambda_{SO}s_z + E^-_{n,s_z,p}}{2E^-_{n,s_z,p}}\right]^{1/2}, \tag{20}$$

$$\eta_2^- = \left[\frac{-\lambda_{SO}s_z + E_{n,s_z,p}^-}{2E_{n,s_z,p}^-}\right]^{1/2}. \tag{21}$$

3. Numerical results and discussion

To have a deeper insight of the above results, we now compute numerically the AP with specified parameters. The following parameters are adopted in the computation [10,37,41,42]: $E_0 = 10^5$ V/m, $v_F = 5.42 \times 10^5$ m s^{-1}, $\lambda_{SO} = 3.9$ meV, $\rho = 7.2 \times 10^{-8}$ g cm^{-2}, and $\hbar\omega_{q,v} = \hbar\omega_0 = 61.2$ meV. Though the energy band structure is inequivalent, the optical absorption in the K and K' valleys is believed to have similar behaviours. Therefore, in the following we only take account of intravalley processes, for example, the K valley will be considered in the numerical calculation.

In Fig. 1, the AP is shown as a function of the photon energy at two values of the magnetic field strength of 5 T (the solid curve) and of 10 T (the dashed curve). We can see clearly the appearance of absorption peaks in each curve. By numerical analysis, we find that these peaks arise from certain conditions which are shown in details as follows. For instance, for the curve with $B = 5$ T, one can show that:

– The left peak locates at the photon energy of 45.3175 meV which satisfies the condition $E_{2,1,1} - E_{1,1,-1} - \hbar\omega_0 = \hbar\omega$, where $E_{2,1,1} - E_{1,1,-1} = 106.5170$ meV. This condition implies the excitation of electrons from state $|1, 1, -1\rangle$ to state $|2, 1, 1\rangle$ by absorbing simultaneously a photon of energy 45.3175 meV and an optical phonon of energy 61.2 meV.

– The right peak occurs at the photon energy of 167.717 meV arising the condition $E_{2,1,1} - E_{1,1,-1} + \hbar\omega_0 = \hbar\omega$. This condition implies the jump of electrons from the state $|1, 1, -1\rangle$ to the state $|2, 1, 1\rangle$ by absorbing a photon of energy 167.717 meV and emitting an optical phonon of energy 61.2 meV.

Two peaks on the curve for $B = 10$ T can be explained similarly where the left and the right peak are, respectively, for phonon absorption and phonon emission. From the above conditions for the peaks, we see that they are the CPR peaks in silicene monolayer where both phonon absorption and emission occur during electron transition induced by the EMW absorption. Practically, both CR and CPR can be applied to determine the effective mass of carrier, the optical phonon energy, and some other parameters in solids (see, for example Ref. [43] and references therein). Recall that in silicene monolayer the cyclotron frequency is given by $\omega_c = \sqrt{2}v_F/\ell_B$ with $\ell_B = \sqrt{\hbar/eB}$. Hence, it is evident that when the CPR condition is achieved, namely $\hbar\omega$ is given, one can obtain experimentally the Fermi velocity (v_F) in this material if the optical phonon energy is known, and vice versa.

To see clearly the variation of the CPR photon energy (or CPR energy, for simplicity) with the static magnetic field strength, in Fig. 2 we show the plot of the CPR energy versus the magnetic field strength for both phonon absorption and phonon emission processes. We can see from the figure that the CPR energy is linearly proportional to the square root of magnetic field strength. This dependence can be explained by the fact that the CPR energy depends linearly on the separation between Landau levels which is proportional to $\sqrt{B}$, i.e, CPR energy $\sim (E_\alpha - E_\beta) \sim \sqrt{B}$. This relation is similar to that in graphene monolayer [29,30,44,45], but different from that in monolayer MoS$_2$ [32] and conventional low-dimensional semiconductors where the CPR energy is proportional to B.

When analysing an absorption spectrum, the full width at half maximum (FWHM) of resonant peaks is a parameter of particular interest. The FWHM gives us information about the mechanism of the resonant absorption. It is known that the FWHM is proportional to the probability of resonant scattering of charged carriers (electrons, holes) with other particles. The effects of magnetic field strength and temperature on the FWHM are usually objects of interest.

To examine the impact of the magnetic field strength on the FWHM of CPR in this study, we consider again the CPR maxima presented in Fig. 1. Adopting the familiar profile method [30,32,46], we can compute the FWHM and show its dependence on the magnetic field strength in Fig. 3. From this figure we can see that when increasing magnetic field strength the FWHM increases and obeys the laws FWHM[meV]=$0.1489\sqrt{B}$ and FWHM[meV]=$0.1430\sqrt{B}$ for phonon emission and phonon absorption, respectively, where B is measured in Tesla. The $\sqrt{B}$-dependent FWHM obtained in this calculation is similar to those observed in graphene [17,18,30] and monolayer MoS$_2$ [32]. However, the FWHM in silicene here is about two times smaller than it is in graphene [18,29,30,44,45] and has the same order of value as it does in monolayer MoS$_2$ [32]. Interestingly, for any magnetic field strength, the FWHM for phonon absorption is always smaller than that for phonon emission. The origin of this behaviour can be explained similarly as in monolayer MoS$_2$ [32] and semiconductor quantum wells [47–51].

We now go forward to examine the influence of temperature on the CPR in the material. In Fig. 4 we show again the AP as a function of the photon energy but for two different values of temperature. We can see that the height and the width of CPR peaks change with temperature but the photon energy at maxima does not depend on the temperature. This behaviour verifies the temperature independence of the above CPR conditions. Furthermore, the variation of the FWHM versus temperature is obtained and introduced in Fig. 5. It is seen from the figure that the FWHM for phonon absorption/emission increases from about 0.167 meV/0.230 meV to 0.390 meV/0.392 meV when increasing temperature from 50 K to 400 K. In this range of temperature, the best fit gives us the laws for the temperature-dependent FWHM to be FWHM[meV]=$0.1305 + 0.0128T^{1/2}$ for phonon emission and FWHM[meV]=$0.0437 + 0.0174T^{1/2}$ for phonon absorption, where T is measured in Kelvin. Interestingly, at high temperatures ($T > 300$ K) the difference between the FWHMs for both cases is not considerable. This is reasonable because the FWHM is proportional to the width parameters $\gamma_{\alpha,\beta}^\pm$ given by Eq. (19) which depends on ($N_{q,v} + 1$) for the former and on $N_{q,v}$ for the latter. At relatively high temperature $N_{q,v} \gg 1$ so ($N_{q,v} + 1$) $\approx N_{q,v}$, and so the FWHMs for both phonon emission and phonon absorption differ not much.

The slight increase of the FWHM with temperature indicates the difference of the effect in graphene and silicene. In graphene monolayer, the FWHM has been calculated and shown to be nearly unchanged with temperature [30]. Besides, it has been shown for monolayer MoS$_2$ [31,32] that the FWHM also increases with increasing temperature in which the increasing rate is larger than it is in silicene. This property shows that the sensitivity to the temperature change of the lattice vibrations (phonons) in silicene is larger than it is in graphene and smaller than it is in monolayer MoS2.
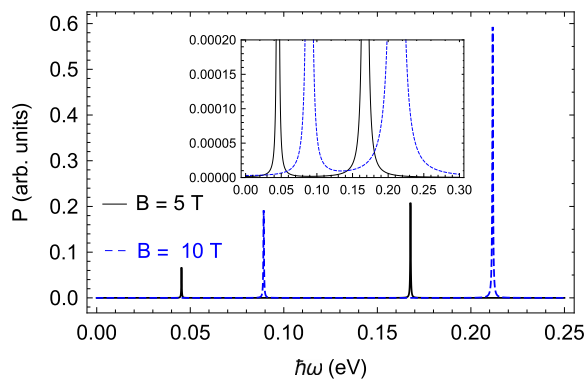
Fig. 1. The AP as a function of the photon energy at two values of the magnetic field strength: $B = 5$ T (the solid curve) and $B = 10$ T (the dashed curve). Here, $T = 250$ K.
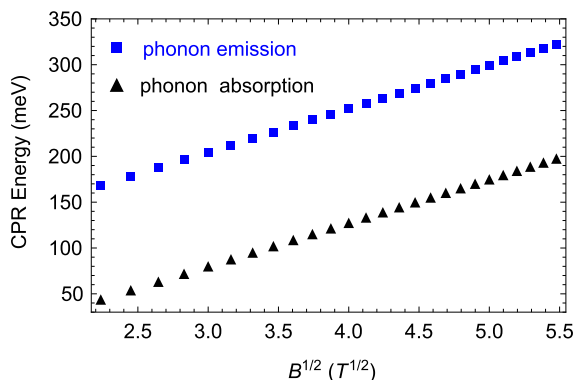

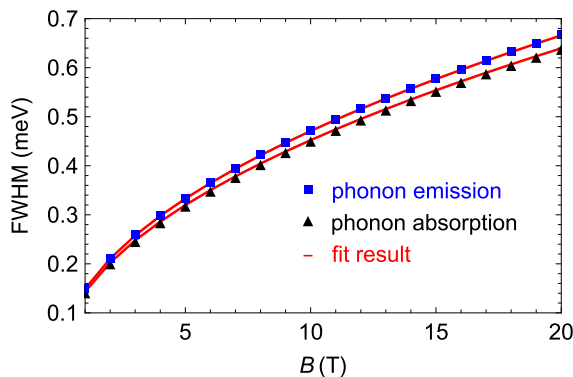**Fig. 2.** The CPR energy versus the square root of magnetic field strength at $T = 250$ K.

Fig. 3. The dependence of FWHM on magnetic field strength at $T = 250$ K. The red solid curves present the fit results.

4. Concluding remarks

We have investigated systematically the optical absorption in a free-standing monolayer silicene in a perpendicular magnetic field. The electron–optical phonon scattering is assumed to be dominant and taken into account at high temperatures. Numerical consideration for the AP shows the CPR effect in which both the absorbing and emitting pf an optical phonon occur. The CPR photon energy depends linearly on the square root of magnetic field strength. This behaviour is similar to that in graphene and different from that in monolayer MoS_2 and traditional low-dimensional semiconductor systems. The profile of the CPR is obtained by calculating computationally the FWHM of the resonant peaks. The dependence of the FWHM on the magnetic field strength has the laws similar to those obtained for graphene and monolayer MoS_2 but with a different coefficient. However, the value of the FWHM in silicene is smaller than it is in graphene and has the same order as it does in monolayer MoS_2. At very high temperature,

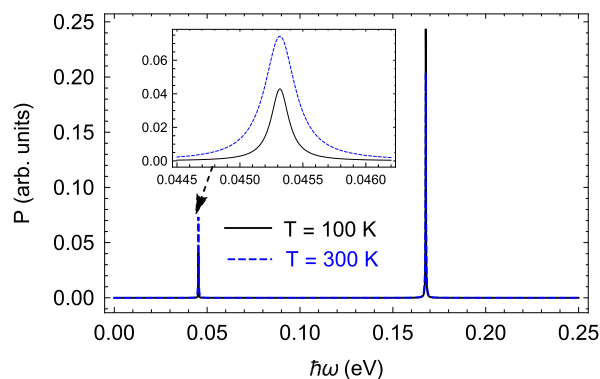**Fig. 4.** The AP as a function of the photon energy at two values of temperature: *T* = 100 K (the solid curve) and *T* = 300 K (the dashed curve). Here, *B* = 5 T.
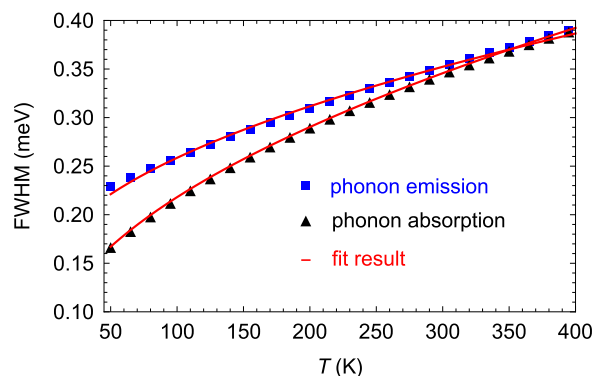

Fig. 5. The variation of FWHM with temperature at *B* = 5 T. The red solid curves present the fit results.

the FWHMs for phonon absorption and phonon emission become identical. So far, there has been no experimental observation of the effect in silicene so that we can compare the present calculation with. However, our results could be a guidance for studying further magneto-optical behaviours in silicene monolayers and possibility of application of the material to nanoelectronic devices.

Acknowledgement

References

[1] Michelle J.S. Spencer, Tetsuya Morishita (Eds.), Silicene: Structure, properties and applications, in: Springer Series in Materials Science, vol. 235, Springer, 2016.
[2] Gian G. Guzmán-Verri, L.C. Lew Yan Voon, Phys. Rev. B 76 (2007) 075131.
[3] P. Vogt, et al., Phys. Rev. Lett. 108 (2012) 155501.
[4] B. Augray, A. Kara, S.B. Vizzini, H. Oughaldou, C. LéAndri, B. Ealet, G. Le Lay, Appl. Phys. Lett. 96 (2010) 183102.
[5] A. Fleurence, R. Friedlein, T. Ozaki, H. Kawai, Y. Wang, Y. Takamura, Phys. Rev. Lett. 108 (2012) 245501.
[6] L. Meng, Y. Wang, L. Zhang, S. Du, R. Wu, L. Li, Y. Zhang, G. Li, H. Zhou, W.A. Hofer, M.J. Gao, Nano Lett. 13 (2013) 685.
[7] Meng Lei, et al., Chin. Phys. B 24 (2015) 086803.
[8] Q. Tang, Z. Zhou, Prog. Mater. Sci. 58 (2013) 1244.
[9] Xiaodong Li, Jeffrey T. Mullen, Zhenghe Jin, Kostyantyn M. Borysenko, M. Buongiorno Nardelli, Ki Wook Kim, Phys. Rev. B 87 (2013) 115418.
[10] Cheng-Cheng Liu, Wanxiang Feng, Yugui Yao, Phys. Rev. Lett. 107 (2011) 076802.
[11] J.S. Bhat, S.S. Kubakaddi, B.G. Mulimani, J. Appl. Phys. 70 (1991) 2216.
[12] J.S. Bhat, B.G. Mulimani, S.S. Kubakaddi, Phys. Rev. B 49 (1994) 16459.
[13] F.G. Bass, I.B. Levinson, Zh. Eksp. Teor. Fiz. 49 (1965) 914.
[14] V.I. Ivanov-Omskii, L.I. Korovin, E.M. Shereghii, Phys. Status Solidi b 90 (1978) 11.
[15] B. Tanatar, M. Singh, Phys. Rev. B 42 (1990) 3077.
[16] Huynh VinhPhuc, Nguyen Dinh Hien, Le Dinh, Tran Cong Phong, Superlattices Microstruct. 94 (2016) 51.
[17] Huynh Vinh Phuc, Le Dinh, Mater. Chem. Phys. 163 (2015) 116.
[18] Huynh Vinh Phuc, Nguyen Ngoc Hieu, Opt. Commun. 344 (2015) 12.
[19] A. Suzuki, D. Dunn, Phys. Rev. B 25 (1982) 7754.

[20] M.P. Chaubey, C.M. Van Vliet, Phys. Rev. B 34 (1986) 3932.
[21] R.J. Nicholas, et al., Phys. Rev. B 45 (1992) 12144(R).
[22] N.L. Kang, et al., J. Phys.: Condens. Matter 7 (1995) 8629.
[23] Y.J. Cho, N.L. Kang, K.S. Bae, J.Y. Ryu, S.D. Choi, J. Phys.: Condens. Matter 8 (1996) 6957.
[24] W. Xu, C. Zhang, Phys. Rev. B 54 (1996) 4907.
[25] S.C. Lee, H.S. Ahn, D.S. Kang, S.O. Lee, S.W. Kim, Phys. Rev. B 67 (2003) 115342.
[26] S.C. Lee, J. Korean Phys. Soc. 51 (2007) 1979.
[27] X.G. Wu, F.M. Peeters, Y.J. Wang, B.D. McCombe, Phys. Rev. Lett. 84 (2000) 4934.
[28] W.Y. Wang, W. Xu, Phys. Rev. B 86 (2012) 045307.
[29] M. Orlita, et al., Phys. Rev. Lett. 101 (2008) 267601.
[30] Bui Dinh Hoi, Le Thi Thu Phuong, Tran Cong Phong, J. Appl. Phys. 123 (2018) 094303.
[31] Chuong V. Nguyen, Nguyen N. Hieu, Nikolai A. Poklonski, Victor V. Ilyasov, Le Dinh, Tran C. Phong, Luong V. Tung, Huynh V. Phuc, Phys. Rev. B 96 (2017) 125411.
[32] N.V.Q. Binh et. al, J. Phys. Chem. Solids 125 (2019) 74.
[33] P. Chantngarm, K. Yamada, B. Soodchomshom, J. Magn. Magn. Mater. 429 (2017) 16.
[34] E. Cinquanta, et al., Phys. Rev. B 92 (2015) 165427.
[35] C.J. Tabert, E.J. Nicol, Phys. Rev. Lett. 110 (2013) 197402.
[36] Y.J. Cho, S.D. Choi, Phys. Rev. B 47 (1993) 9273.
[37] Kh. Shakouri, P. Vasilopoulos, V. Vargiamidis, F.M. Peeters, Phys. Rev. B 90 (2014) 125444.
[38] M. Ezawa, Phys. Rev. Lett. 109 (2012) 055502.
[39] Jiseok Kim, Massimo V. Fischetti, Shela Aboud, Phys. Rev. B 86 (2012) 205323.
[40] M.P. Chaubey, C.M. Van Vliet, Phys. Rev. B 33 (1986) 5617.
[41] C.-C. Liu, H. Jiang, Y. Yao, Phys. Rev. B 84 (2011) 195430.
[42] M.V. Fischetti, S.E. Laux, J. Appl. Phys. 80 (1996) 2234.
[43] D.J. Hilton, T. Arikawa, J. Kono, Cyclotron resonance, in: Elton N. Kaufmann (Ed.), Characterization of Materials, John Wiley & Sons, Inc., 2002.
[44] Z. Jiang, E.A. Henriksen, L.C. Tung, Y.-J. Wang, M.E. Schwartz, M.Y. Han, P. Kim, H.L. Stormer, Phys. Rev. Lett. 98 (2007) 197403.
[45] C.H. Yang, F.M. Peeters, W. Xu, Phys. Rev. B 82 (2010) 205428.
[46] Le T.T. Phuong, Huynh V. Phuc, Tran C. Phong, Physica E 56 (2014) 102.
[47] Khang D. Pham, Le Dinh, Chuong V. Nguyen, Nguyen N. Hieu, Pham T. Vinh, Le Thi Ngoc Tu, Huynh V. Phuc, Appl. Phys. A 25 (2019) 166.
[48] Khang D. Pham, Nguyen N. Hieu, Le T.T. Phuong, Bui D. Hoi, Chuong V. Nguyen, Huynh V. Phuc, Appl. Phys. A 124 (2018) 656.
[49] Doan Q. Khoa, et al., Optik 173 (2018) 263.
[50] Khang D. Pham, Le Dinh, Pham T. Vinh, C.A. Duque, Huynh V. Phuc, Chuong V. Nguyen, Superlattices Microstruct. 120 (2018) 738.
[51] Luong V. Tung, Pham T. Vinh, Huynh V. Phuc, Physica B 539 (2018) 117.